ESA Climate Space Tipping Elements Project

RESET lakes

Scientific Methodology and Feasibility

Deliverable 2.1 Version 1.1

13 May 2026

Authors

Caren Binding

Laura Boyall

Elisa Calamita

Daniel Odermatt

Luiz Oliveira

Ann Scheliga

Iestyn Woolway

Christiane Zarfl

eawag aquatic research

Prifysgol Bangor University

Environment and Climate Change Canada / Environnement et Changement climatique Canada

Eberhard Karls Universität Tübingen

Content

1 Purpose

In this document, we provide an initial description of methodology and feasibility for the scientific analysis of lake tipping points using Earth Observation (EO) products. The potential for using EO data is strongly influenced by spatial and temporal availability, consistency, and uncertainties. The focus here is on quality assessment methods, and results are reported for feasibility assessments. The methods for lake modelling and tipping point identification are presented here as a methodological framework that can be adjusted during the upcoming experimentation phase.

The EO product quality assessment is described in Section 2, including references for the algorithms and retrieval methods used to develop these existing EO products. This review focuses initially on data services available from the ESA Climate Change Initiative (CCI) for lakes and is thus the basis for providing feedback to the corresponding CCI team. As we expand the analyses, data quality assessment methods for other sources will be added. Section 3 is a placeholder in case we need to define the development of additional EO data products. In Section 4, we describe the lake model we use, the simulations and projections we run with the model, and how the lake model and EO-based analyses will complement each other. In Section 5, we define the generic tipping point detection metrics we use, and which we expect to be aligned with those used by the other CCI Tipping Point projects. We further elaborate on considerations specific to lakes. In Section 6, we exemplify our methodological approach using a case study on Great Bear Lake.

We have not yet needed to implement our own EO retrieval algorithms, but we include Section 3 on implementation of EO retrieval algorithms to highlight our capacity to perform retrieval work should we identify a need. Version 2 of this document will be submitted as part of the Analysis and Validation Review in 12 months.

2 Quality assessment of operational EO products

In this section, we assess the data quality of the EO products we have used thus far in the project. The list of variables is not exhaustive and will be complemented with additional CCI variables as the project continues. We report on assessments of temporal coverage, spatial coverage, and inter-sensor consistency of each variable, and describe how these properties influence our ability to detect lake tipping points. In selected cases, we use in situ measurements to validate the CCI products.

From the Lake CCI dataset, we cover Lake Surface Water Temperature (LSWT, Section 2.1), chlorophyll-*a* (chl-*a*, Section 2.2), and the upcoming phytoplankton and cyanobacteria phenology (Section 2.3). The ESA Lakes CCI products nominally provide daily observations for 2,024 lakes worldwide, with a spatial resolution of 1/120° (approximately 1 km at the equator) [Carrea et al., 2024].

We also describe alternative chl-*a* products from OC CCI and a lake stratification product developed for a previous ESA project, LakeCREST, based on Lake CCI LSWT products (Section 2.4).

2.1 Lake surface water temperature

The Lake CCI LSWT product combines brightness temperature retrievals from multiple satellites and expected LSWT from a radiative transfer model to create a single harmonized data product. The radiative transfer model uses atmospheric reanalysis variables, prior LSWT, and total water column vapor to determine the expected LSWT [MacCallum & Merchant 2012].

Coverage in time

The LSWT product has a nominal temporal coverage of 1995-2022 in v2.1 (to 2023 in v3.0). However, there is a global gap in the data product for the first half of 1996. The LSWT data product contains missing values throughout the time series. The data gaps are most notable in the early time series, before 2000. The RESETlakes project team has access to a gap-filled LSWT dataset from the LakeCREST project. We will review the upcoming gap filled LSWT by the Lake CCI team as soon as it is completed.

Consistency over sensors

The LSWT product is derived from several satellites and meteorological reanalysis products using an optimal estimator scheme. Figure 1 shows the temporal coverage of the satellite sensors. The LSWT optimal estimator scheme produces sensitivity and goodness of fit descriptors that are then used to determine the quality level of the LSWT retrieval. The grid cell LSWT for a given day is selected by averaging the highest quality retrieval(s) available that occur in the grid cell space. With this harmonization method, the final product incorporates data from all available sensors.

From our initial analysis, the ATSR2-only period (1995-2001) tends to have more data gaps, higher autocorrelation, and lower variance than later multi-sensor periods. This distinct statistical behaviour would influence tipping point detection but given the shorter temporal coverage of complementary datasets (i.e. Lake CCI chl-*a*) and that candidate tipping points near the end of a time series are not significant, we do not believe this will impact our ability to use LSWT for tipping point detection. Additionally, from the Lake CCI product validation report, the median difference between satellite and in-situ temperatures is consistent (and small) for high quality pixels throughout the time frame [Simis et al. PVIR 2025].

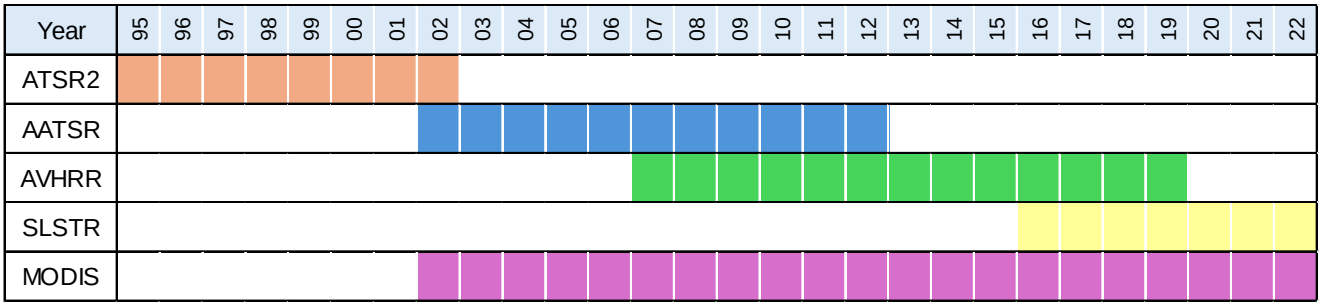

Figure 1: Temporal coverage of satellite sensors for the Lake CCI LSWT product (v2.1), based on table in Simis et al. PVIR 2025.

Spatial consistency

Lake ice cover is a major source of spatial variability in the LSWT product. Ice-covered surface water is currently filled with NaN in the Lake CCI LSWT product, i.e., it appears as a data gap while the state of the water surface is known but cannot be expressed in terms of LSWT. Choosing a different convention, our internal gap filling product prescribes the LSWT as 0°C when (i) LIC product shows ice is present, (ii) LSWT is missing data for that day, and (iii) the pixel's climatology for that day is below 4°C. The Lake CCI team is working to incorporate a combined LIC-LSWT processing chain to achieve a similar gap filling framework.

2.2 Chlorophyll-*a*

CCI chl-*a* products are available for Lakes CCI on one hand, but also from Ocean Colour CCI v6.0 (OC CCI) for some of the largest inland seas and lakes. The Lakes CCI chl-*a* and corresponding lake water-leaving reflectance (LWLR) spectra are processed with *Calimnos*, a multi-step processing chain that handles pixel identification, atmospheric correction, optical water type (OWT) classification and blending, and calculation of derived products (i.e. chl-*a*) [Simis et al. ATBD 2025]. OC CCI and Lake CCI use the same OWT fuzzy logic classification scheme [Moore et al. 2001]. The OC CCI product uses the POLYMER algorithm for pixel identification and atmospheric correction [Groom et al. 2024]. Then, as OC CCI uses multiple sensors over the same timeframe, the signals for a single pixel are band-shifted, bias-corrected and averaged. Chl-*a* is calculated with different algorithms based on the sensor (for Lake CCI) and optical water type classification [Groom et al. 2025, Simis et al. ATBD 2025].

We compare the OC CCI and Lakes CCI chl-*a* products against in-situ observations over the Laurentian Great Lakes to assess the product continuity across multiple satellite missions. We completed the comparison for version 2.1 of the Lake CCI product and have preliminary results for v3.0. We use in-situ samples taken at depths of < 5m. Figure 2 shows the locations of in-situ sampling sites. The OC CCI and in-situ sites have 2551 matchups from 1998 through 2024, the Lake CCI v2.1 has 1364 matchups from 2002 through 2022, and Lake CCI v3.0 has 1116 matchups from 2002 through 2023. Note that there are no in-situ measurements for 2020.

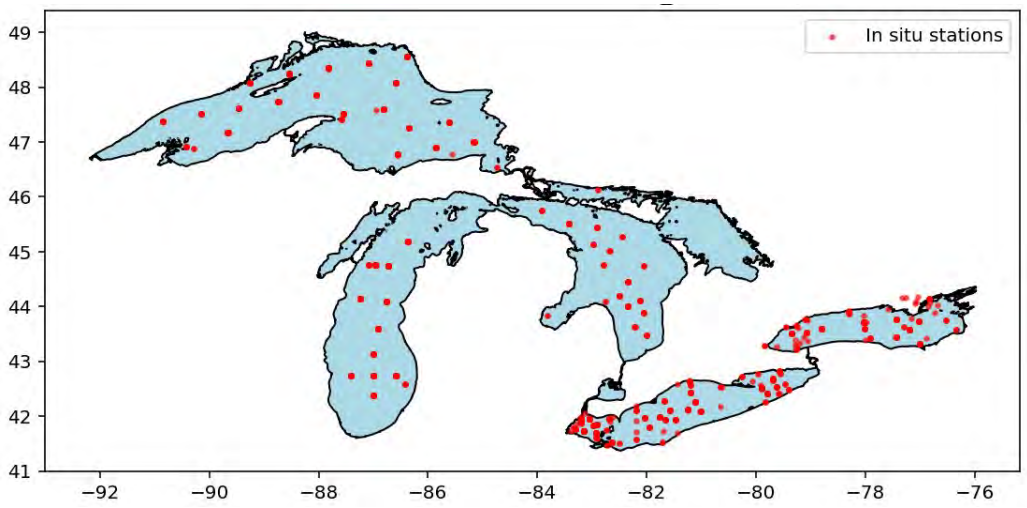

Figure 2: In-situ chl-a sampling sites with OC CCI matchups across the Laurentian Great lakes, acquired via the US EPA GLENDA and ECCC WQMS Great Lakes surveillance programs.

Coverage in time

The Lake CCI chl-*a* product begins in 2002 and ends in 2022 (v3.0 ends in 2023). For most lakes (v2.1: 1976 out of 2024 lakes) in the Lake CCI dataset, there is a four-year gap in LWLR products (including chl-*a* and turbidity) from 2012 into the beginning of 2016. The gap arises because atmospheric corrections are more challenging when relying solely on MODIS observations [Liu et al., 2024]. For 48 lakes (in v2.1), the 2012-2016 gap is filled with MODIS data. As shown in Figure 3, the Lake CCI product is derived from the MERIS instrument on Envisat from 2002-2012, the MODIS sensor on Aqua from 2012-2016 (where applicable), and the OLCI sensor on Sentinel-3 A/B from 2016 onwards [Calmettes et al., 2025]. The Lake CCI product ends in 2022, due to data processing constraints. Successive versions of Lake CCI will extend the time series.

Consistency over sensors

In contrast to the Lake CCI product, which looks at sensors consecutively, the OC CCI product merges overlapping data across multiple sensors when available, including data from the SeaWiFS and VIIRS sensors [Groom et al. 2025]. Since OC CCI uses a simple average to merge data individual sensor data and bias corrects the sensors before merging, inter-sensor shifts are less prominent in the OC CCI time series than in the Lake CCI series.

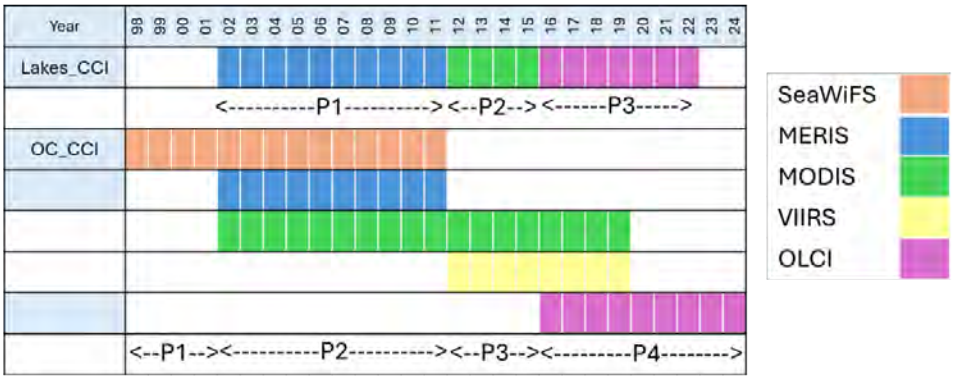

Figure 3: Temporal contributions of satellite sensors to the Lake CCI (v2.1) and OC CCI chl-a data products.

The bias during the MODIS period in Lake CCI (Figure 4) shows a distinctive shift: lower mean bias, but with a large increase in the range. This sensor shift is statistically equivalent to a physical tipping point, severely limiting the utility of the Lake CCI chl-*a* products for tipping point detection. The OC CCI bias (Figure 5), by comparison, has a notable sensor-attributable bias only during the 1998-2001 SeaWiFS period. This sensor bias at the beginning of the time series is less detrimental to our tipping point analysis, because we can simply remove the early, high bias years.

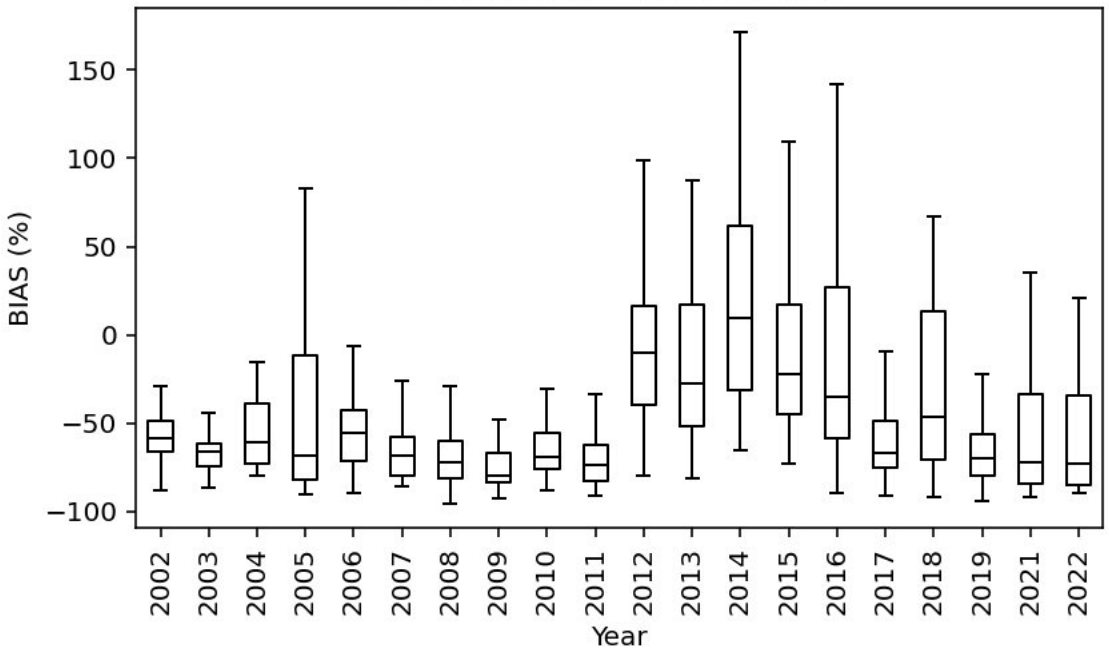

Figure 4: Bias between Lake CCI (v2.1) and in-situ chl-a estimates by year, across the sequence of MERIS (2002-2011), MODIS (2012-2015) and OLCI (2016-2022).

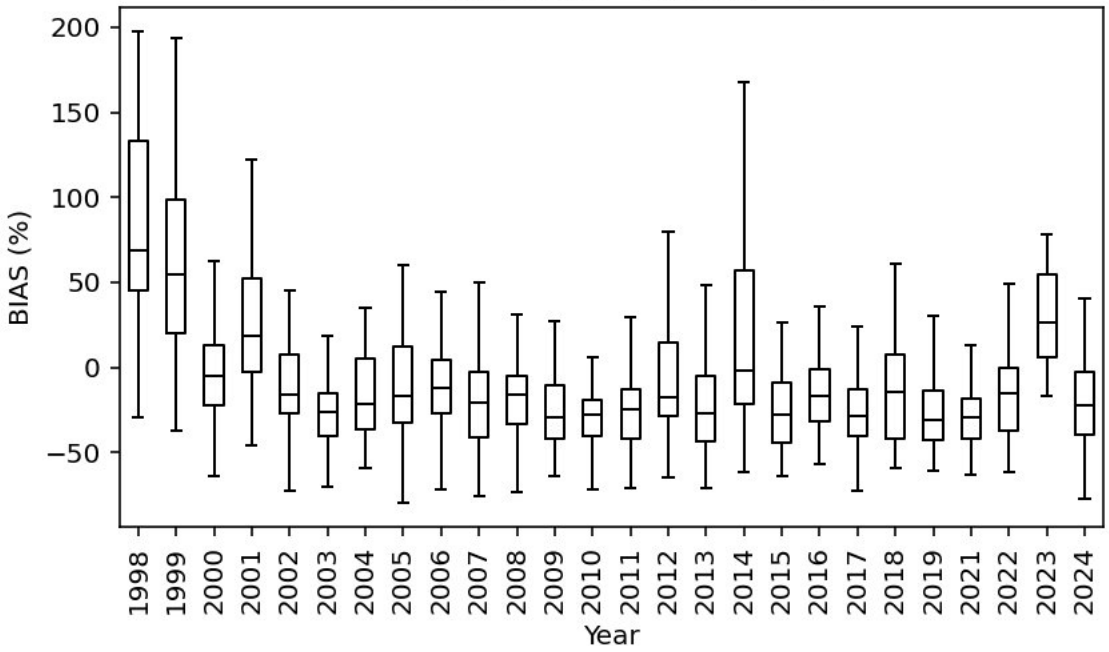

Figure 5: Bias between OC CCI and in-situ chl-a estimates by year, merging retrievals from SeaWiFS, MERIS, MODIS, VIIRS and OLCI data.

Spatial consistency

From our analysis, we find that the Lake CCI v2.1 product has good agreement with in-situ measurements for chl-*a* values greater than ~2 ug/L. However, v2.1 has a strong negative bias for oligotrophic lakes. Version 3.0 data was provided to us very recently and validation is still ongoing. The use of MODIS data in Version 3.0 was reduced due to the addition of a new quality control criterion. This led to some oligotrophic lakes, including Lake Michigan, no longer containing MODIS gap-filled data.

2.3 Phytoplankton phenology

Coverage in time

The Lake CCI phenology products are currently being produced at Eawag, using a method based on cubic spline fitting which was developed in collaboration with Plymouth Marine Laboratory. The fits are applied to the Lake CCI chl-*a* and the new cyanobacteria index time series for each 1km pixel in each lake. Thus, the phytoplankton phenology products have the same nominal temporal coverage as the water quality products from which they are derived. From the cubic spline (Figure 6), we establish the timing of peaks and troughs (local maxima and minima), as well as green up and green down points, like phenology for terrestrial vegetation [Gray et al. 2019]. Mid- and high-latitude lakes tend to have one or two phytoplankton blooms per year, and we can derive typical and anomalous phytoplankton blooms from this muti-year product. Initial analysis indicates low-latitude lakes are more likely to have more than two blooms per year.

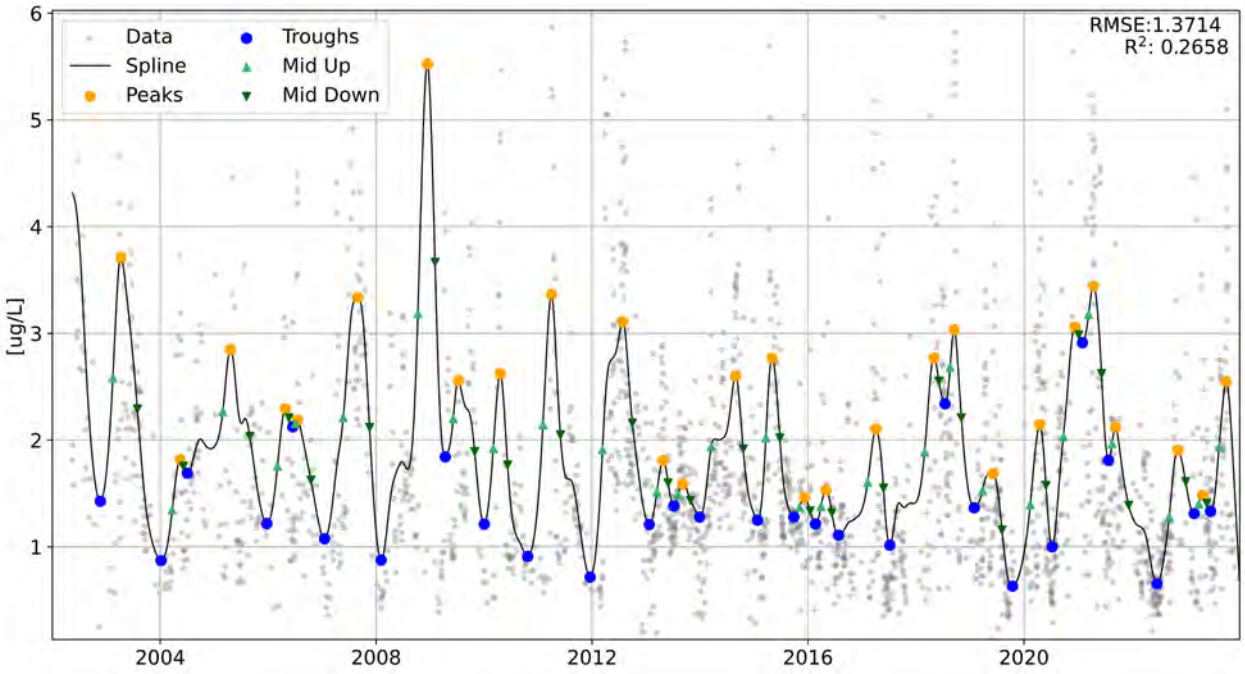

Figure 6: Chlorophyll-a (grey points) and phenology product from Lake CCI v3.0 for a pixel in Lake Geneva. Peaks (yellow dots), troughs (blue dots), green up midpoints (light green triangles), and green down midpoints (dark green triangles) are isolated from the cubic spline (black line).

Consistency over sensors

As with the underlying water quality products, the phytoplankton phenology products are also sensitive to sensor bias (Figure 7). Most lakes have a data gap from 2012 to 2016, and the time series for pre-2012 (MERIS) and post-2016 (OLCI) time series have distinct ranges of values, as shown in the phycocyanin product in Figure 7. However, as the phenology products focus on the timing of chl-*a* more than on absolute magnitude, we must further investigate if we can perform inter-sensor temporal analysis on the phenology product with more confidence than on the underlying chl-*a* product.

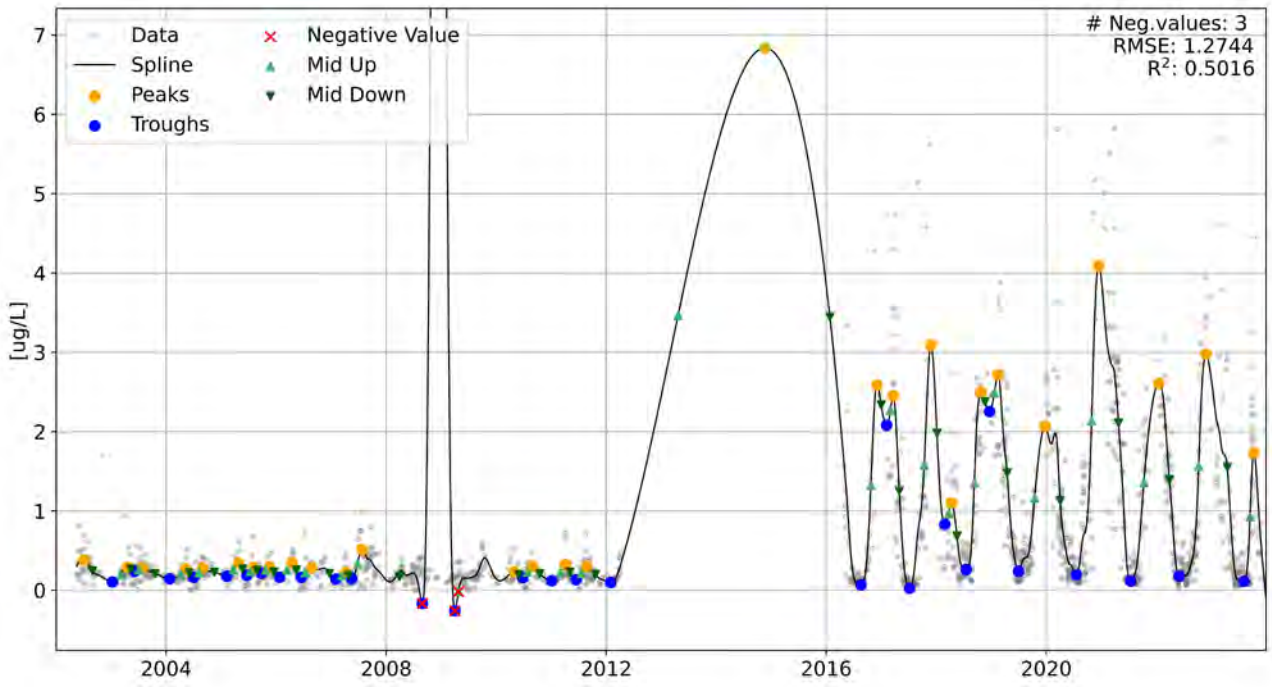

Figure 7: Phycocyanin (grey points) and phenology product from Lake CCI v3.0 for a pixel in Lake Geneva. Peaks (yellow dots), troughs (blue dots), green up midpoints (light green triangles), and green down midpoints (dark green triangles) are isolated from the cubic spline (black line).

Spatial consistency

By aggregating the per-pixel phenology terms, we can assess the extent and duration of phytoplankton blooms within a given lake (see previous work by Eawag and Lake CCI team members[1]).

2.4 Stratification and mixing

Coverage in time

We define the stratification and overturning cycles for lakes using a Mixing Cycle Identification (MixCI) framework developed within the ESA project LakeCREST [Calamita et al., in revision]. The MixCI analysis uses gap-filled LSWT to detect thermal bars and determine typical mixing patterns for a given lake. Thus, the product covers the same time frame as the Lake CCI LSWT product.

Consistency over sensors

The MixCI product is consistent across satellite sensors, as it is derived from the Lake CCI LSWT product which has been shown to be consistent across sensors [Simis et al. PVIR 2025]. We do not anticipate major corrections to account for sensor bias or shifts.

[1] current version at https://lakephytoplanktonphenology.earth/. Temporary restriction requires login: lake, password: phenology

Spatial consistency

The MixCI framework has mainly been applied to dimictic lakes that shift towards warm monomictic behaviour (Calamita et al., in revision), and cold monomictic lakes that may become dimictic (see Section 6.2). Climate regions without regular winter mixing (i.e. low-latitudes or low-altitudes) are outside the scope of this product. On product level, MixCI is based on the ratio of lake area with water temperatures above and below 4°C, i.e., the temperature of maximum density, which was successfully retrieved from gap filled LSWT products.

3 Implementation of EO retrieval algorithms

We have not yet implemented any new EO retrieval algorithms for the project. We have focused our analysis on the published Lake CCI products and recently developed algorithms for lake stratification and phytoplankton phenology retrievals.

4 Lake modelling

Whilst satellite observations provide an unparalleled, spatially extensive record of recent lake surface conditions, they are intrinsically limited in their ability to (i) resolve sub surface processes, (ii) isolate physical mechanisms driving the observed changes, and (iii) assess long-term or future system behaviour under changing climates. To address these limitations, process-based lake models can be incorporated as a complementary line of evidence.

4.1 ISIMIP and model choice

The Inter-Sectoral Impact Model Intercomparison Project (ISIMIP) is an internationally coordinated modelling framework designed to systematically assess the impacts of climate change across multiple interacting components of the Earth system [Golub et al., 2022]. ISIMIP brings together modelling groups from a wide range of impact sectors including water resources, agriculture, ecosystems, health, and inland waters under a common experimental protocol.

Central to ISIMIP is the use of stringent, standardized modelling guidelines, which specify climate forcing datasets, bias-correction methods, spatial and temporal resolutions, scenario design, and output variables. These protocols ensure that simulations produced by different models and sectors are directly comparable, enabling robust attribution of impacts to climate forcing rather than to methodological differences among models. Within the RESETlakes project, we follow the ISIMIP protocol and use the lake models simulated under these guidelines. In particular, we use the latest version of the ISIMIP protocol[2] – ISIMIP3b, providing detailed information about each experiment run, forcing data, file formats and output data. It focuses on not only the historical period but also on future projections of changing lake processes until the end of the century with changing socioeconomic conditions.

Other model intercomparison projects are available, notably the Tipping Points Modelling Intercomparison Project (TIPMIP). TIPMIP aims to advance the understanding of tipping in different Earth systems using some of the latest Earth system models. However, this intercomparison project is currently in its infancy, with many of the protocols for the different modelling experiments not yet published. Importantly, there is currently no Earth system division within this project relating directly to

[2] https://protocol.isimip.org/#/ISIMIP3b/lakes_global (last accessed 3rd March 2026)

lakes or internal waters. We would therefore need to develop new protocols for lake-based experiments, which is beyond the scope of the RESETLakes work. As a result, RESETLakes will use the ISIMIP project for model guidelines, but will maintain dialogue with the TIPMIP project for possible future collaboration or alignment.

4.2 ALBM modelling

Despite there being several process-based lake models available under the ISIMIP3b protocol, we chose Advanced Lake Biogeochemistry Model (ALBM) version 3.0 [Tan et al., 2024]. This lake model was first initially developed for Arctic lakes but was later found to be adaptable to temperate lakes, making it a suitable model for a global investigation. ALBM is one of two lake models available in the ISIMIP3b global database with the other being the General Ocean Turbulence Model (GOTM, Sachse et al., 2014). GOTM was built for oceans and later adapted to lakes, which is why we consider it less suited for the objectives of RESETlakes. The spatial grid of the ALBM simulations is 0.5' x 0.5' and it produces daily estimates of lake processes. The available output files are as follows: bottom temperature, ice thickness, latent heat flux, lake heat flux, upward longwave radiation, sediment heat flux, sensible heat flux, surface temperature, and water temperature.

Input data

Under the ISIMIP framework there are five models used: MRI-ESM2-0, IPSL-CM6A-LR, MPI-ESM1-2-HR, UKESM1-0-LL, and GFDL-ESM4. Each of these models uses their own input variables to simulate the lake conditions, of which the climate data are bias-corrected projections of climate from the Coupled Model Intercomparison Project (CMIP6). The climate input variables are as follows: near-surface relative humidity, near-surface wind speed, surface temperature (minimum, mean and maximum), shortwave downwelling radiation, snowfall, surface air pressure, and total precipitation. The meteorological drivers are uni-directional and therefore the interactions from lakes to climate are not considered. The ALBM model simulations were conducted in the historic period (1850-2014) and the climate projections during this period are forced by natural internal and external variability, anthropogenic greenhouse gases, and aerosol forcings.

The second set of simulations relate to the future projections (2015-2100) of lake processes under different forcing scenarios. The Shared Socioeconomic Scenarios (SSPs) represent varying levels of socioeconomic changes relating to levels of, for example, climate change policies and GDP growth. The simulations for RESETlakes use mostly the two endpoint scenarios: SSP1-2.6 which represents the highest levels of mitigation, and SSP5-8.5 which represents the lowest levels of mitigation, and in some cases uses the middle scenario, SSP3-7.0.

In addition to climate data, the simulations input static gridded lake conditions, including the hypsographic volume and area, elevation, depths, volume and surface area [Khazaei et al., 2022; Golub et al., 2022]. The simulations use the HydroLAKES lake mask [Messager et al., 2016] to obtain attribution information for each lake which can then be used to match the lakes in the lake_CCI metadata table. The HydroLAKES database provides shoreline polygons for approximately 1.4 million lakes that have a surface area greater than 10 hectares.

4.3 Model analyses and EO integration

The main limitation of EO data is the limited temporal coverage, especially within the context of early warning tipping detection, which may rely on decades of data. However, this short coverage can be easily mitigated with the integration of models. Within the RESETLakes project, the model simulations mentioned above will be used in combination with the EO data to provide an extension of the temporal

scale into the future. The EO data provides an instrumental understanding of lakes current and past behaviour from the last few decades. Statistical analysis of early warning detection (see Section 5) will be first applied to the EO data. Where this analysis highlights lake characteristics that are demonstrating early warning behaviour, the models can then be used In addition, we can then explore how these systems develop under different forcing scenarios, providing the opportunity to explore whether the early warning behaviours exhibited in the lakes is likely to develop into a full tipping point.

At present, the lake processes and characteristics we focus on with the lake simulations are LSWT, lake mixing regime and the length of the ice season. For analysis relating to the length of ice season, we use the ice thickness simulation and calculate the length of the season using the following definition: >0.1 m of ice present on a lake for more than five consecutive days marks the start of the ice season, and <0.1 m of ice for more than five consecutive days marks the end of the ice season and the start of the ice-free season. These seasons are calculated for each of the historical and scenario projection files (Figure 6).

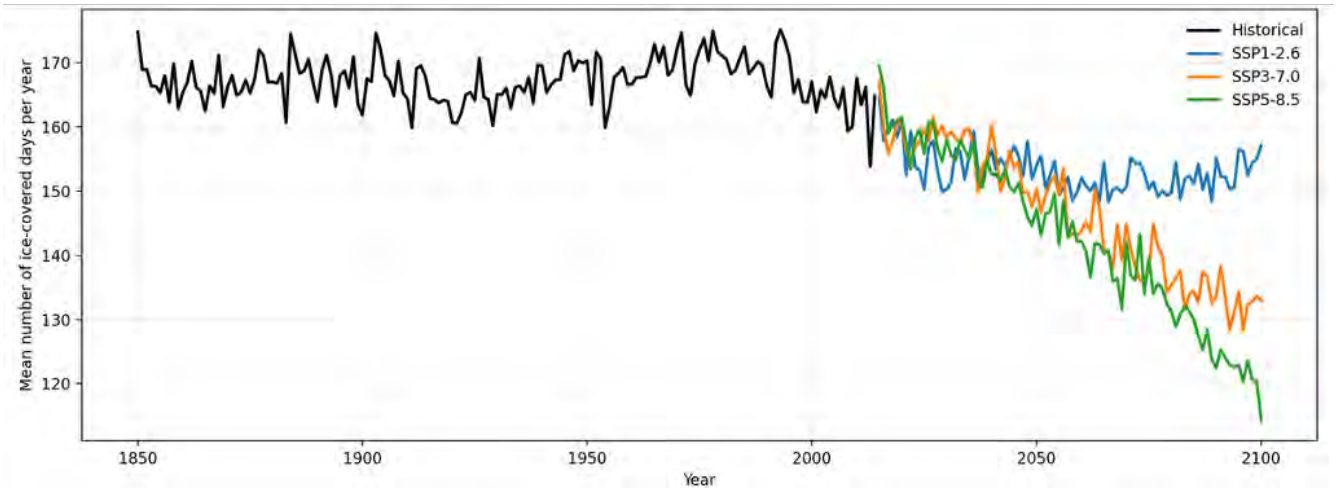

Figure 8: Timeseries of the length of ice season in the past (1850-2014) and future (2015-2100) under the SSP1-2.6, SSP3-7.0 and SSP5-8.5 scenarios for lakes situated 30-90N.

For the categorization and analysis of the lake mixing regimes we use the bottom and surface water temperature, and the ice thickness simulations. We follow the mixing regime classifications of Woolway and Merchant (2019) to classify each of the globally simulated lakes into nine mixing regimes. As it is possible that the mixing regimes change through time, especially through the scenario projection period we classify a baseline period between 1981-2010 where we identify the mixing regime of each lake though this period and then explore the deviance from this period. Figure 7 shows the simulated categorized mixing regimes for lakes between 30-90N during the baseline period.

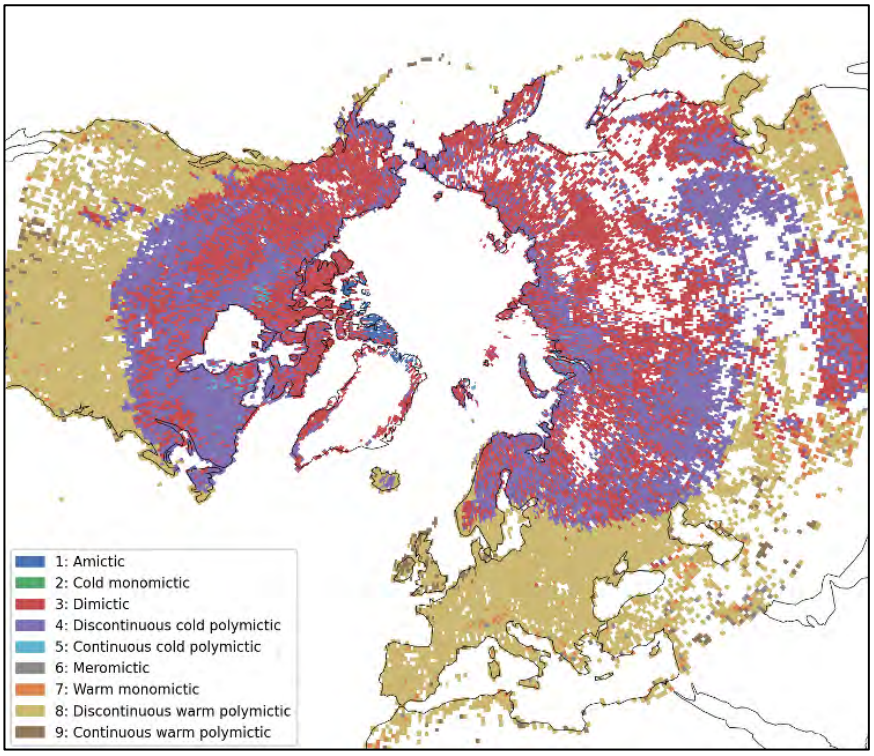

Figure 9: Simulated lake mixing regimes for the 1981-2010 reference period for the ALBM model for lakes 30-90N. Classifications are defined according to Woolway and Merchant (2019).

5 Tipping point detection

5.1 Definitions

A tipping point must typically meet the following criteria: (1) be self-perpetuating, (2) be irreversible, (3) be abrupt for a given timescale, and (4) have an outsized spatial scale and impact [Armstrong McKay et al. 2022].

To assess self-perpetuation and irreversibility, we will run model simulations of future warming and subsequent cooling to determine if the lakes return to their original states. Additionally, we plan to consider reversible or non-catastrophic tipping elements.

The existing definition of abruptness within climate science is that an abrupt change occurs over a few decades or less and persists for at least a few decades [Lenton et al. 2008, Armstrong McKay et al. 2022]. In addition, as lakes are an understudied tipping element [Loriani et al. 2025], we have the option to determine if other detection methods are more appropriate for lakes, such as edge-detection abruptness based on standard deviation as used in Gilarranz et al. 2022.

For spatial scale and impact, we take a catchment and global approach. Lakes are known “sentinels of changes” within their watershed, as changes in the upstream catchment can have an outsized impact on the lake. Our global analysis will allow us to determine if lakes behave as distributed, synchronous tipping systems (like the synchronous global melting of glaciers) or part of cascading tipping systems [Levermann et al. 2012, Armstrong McKay et al. 2022, Lenton et al. 2024].

5.2 Statistical indicators

Generic metrics

To determine if a regime shift has occurred in a time series of any lake variable, we look for: breakpoints in the mean, changes in trend, and changes in variance. We use the Pettitt change test to determine breakpoints in the mean of the time series. Once we find a breakpoint, we use a Mann-Kendall non-parametric test to determine if a change in trend is significant [Adrian et al. 2009], and we use non-parametric Sen slope to quantify the magnitude of the trends before and after the breakpoint [Basu et al. 2024]. We also determine significant change in variance across a breakpoint with ANOVA analysis [Basu et al. 2024].

We use a seasonal–trend decomposition based on LOESS (STL) method [Cleveland et al., 1990] to decompose time series into trend, seasonal, and residual components using locally estimated scatterplot smoothing (LOESS) through local polynomial regression, so that we can analyse each component separately.

We will assess the ability of established early warning indicators (EWIs) to detect identified lake tipping points. The established EWIs we will use are increased variance, increased autocorrelation, and increased skewness in a time series [Andersen et al. 2009, Scheffer et al. 2009]. We will investigate which lake variables under which timescales are the best predictors of lake tipping points.

Metrics for overturning and stratification anomalies

In addition to examining traditional early warning indicators, we can also detect categorical anomalies in lake mixing classification associated with regime destabilization [Woolway and Merchant 2019]. We use two sets of tests to determine if a given lake variable is statistically different in anomalous mixing years versus in non-anomalous mixing years.

The two sets of test are: (i) Welch's analysis of variance (ANOVA) followed by the Games-Howell post-hoc test [Games and Howell, 1976], and (ii) the two-sided Mann-Whitney U test. Both methods assume that samples are independent. While the Welch ANOVA accommodates heteroscedasticity and unequal sample sizes, the Mann–Whitney U test is a nonparametric alternative that does not require normality [Lehmann and Romano, 2022]. For both tests, the significance level was set at 0.05. The specific hypotheses tested are summarized in Table 1.

Table 1: Employed hypothesis tests and their hypotheses.

Test	Type	Null hypothesis (H0)	Alternative hypothesis (H1)
Welch's ANOVA	Parametric	All group means are equal	At least one group mean is different
Games-Howell	Post-hoc (pairwise)	The two-group means are equal	The two-group means are different
Two-sided Mann-Whitney U	Non-parametric	The two group medians are equal	The two group medians are different

For the two-sided Mann–Whitney U test, when the null hypothesis was rejected, the probability of superiority (PS) was calculated according to [Eq. 1].

$$PS = \frac{U}{(n_{anomalous} \cdot n_{non-anomalous})} \quad \text{[Eq. 1]}$$

where U is Mann-Whitney U statistic, $n_{anomalous}$ is the number of anomalous samples and $n_{non-anomalous}$ is the number of non-anomalous years.

The probability of superiority represents the probability that a randomly selected observation from the anomalous group exceeds a randomly selected observation from the non-anomalous group. Under the symmetry condition $PS = 0.5$, the two groups are statistically indistinguishable, corresponding to acceptance of the null hypothesis. Values lower than 0.5 indicate that observations from the anomalous group tend to be smaller than those from the non-anomalous group, whereas values greater than 0.5 indicate the opposite.

5.3 Implementation across EO and model simulations

With a suite of environmental variables, the project will assess cascading tipping and concurrent early warning indicators [Lenton et al. 2022]. Further, by coupling the EO-based detection with the ALBM, we can move from multivariate correlations to process-based understanding.

Without a strong process-based backing, observational studies can only detect “suspected” tipping points [Gilarranz et al. 2022]. We use ALBM projections to assess the irreversibility and persistence of lake shifts. By running cooling experiments, we can determine if shifted lake mixing regimes return to pre-industrial conditions.

6 Great Bear Lake feasibility study

In this case study, we assess how the propagation of thermal anomalies to the biological productivity in a lake can be explored using EO data. We chose Great Bear Lake (GBL) as a demonstrator, but we may expand the analyses to other high-latitude lakes that are shifting from cold monomictic to dimictic behaviour, and use supporting model simulations to verify our findings.

GBL is located in the Northwest Territories of Canada and crosses the Arctic Circle (Figure 8a). The lake bathymetry and the locations of temperature moorings are shown in Figure 8b. GBL has a mean depth of 71 m and a maximum depth of 446 m; its outflow is the Great Bear River, and circulation occurs in a clockwise direction. The lake exhibits low turbidity, allowing the assumption that the effects of salinity and suspended solids on water density are minimal [Carmack et al., 2024]. The lake surface is typically completely frozen from November to May [Kang et al., 2012; Carmack et al., 2024].

GBL generally exhibits a cold monomictic mixing regime; however, over the 22-year period from 2000 to 2022, temperature anomalies temporarily shifted the regime to dimictic conditions [Johnson, 1966; Carmack et al., 2024]. Six anomalous years were previously identified in ESA’s LakeCREST project: 2006, 2010, 2011, 2012, 2016, and 2021.

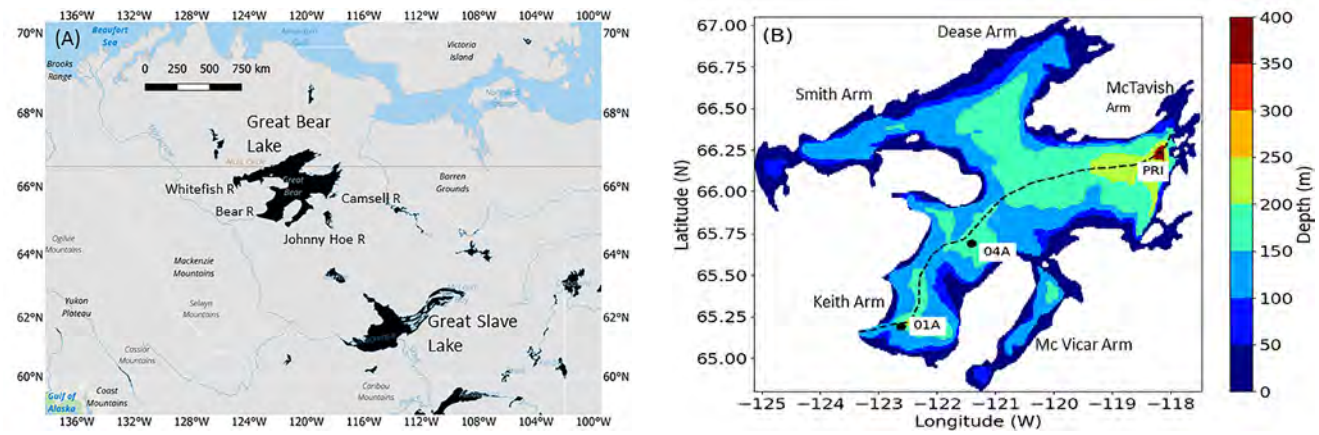

Figure 10: Great Bear Lake's: a) map location and b) bathymetry with mooring locations from Johnson (1966) and modified by Carmack et al. (2024).

6.1 Data pre-processing

In this section, we describe the pre-processing steps applied to the multivariate dataset from GBL. The pre-processing comprises three phases: (i) raw data filtering and time-series truncation; (ii) seasonal–trend decomposition; and (iii) residual filtering and outlier removal.

The time series were truncated to the period from 1 June to 31 October (153 days per year) to account for the lake ice regime, which constrains open-water conditions [Kang et al., 2012; Carmack et al., 2024]. In addition, variables were pre-filtered to remove implausible values based on expected ranges for a cold monomictic, high-latitude lake, see Table 2 for the valid range of each variable. A 1 km buffer (approximately equivalent to one pixel) from the shoreline was further applied to exclude pixels potentially influenced by littoral processes, mixed land–water signals, or edge-related artefacts. Based on lake bathymetry classify the remaining pixels into three spatial domains: (a) entire lake (all pixels), (b) deep areas (Depth > 50 m), and (c) shallow areas (Depth < 50 m).

Table 2: Valid ranges of EO variables for Great Bear Lake

Variable	Minimum	Maximum	Notes
LSWT	0 °C	15 °C	Consistent with the lake's climatology (Figure 12)
Chl-*a*	0 mg/m^3	30 mg/m^3	Expected range for oligotrophic lake

For the STL decomposition, the seasonal period was set to STL_{period} = 153 days to match the number of observations per year in the truncated time series, and the seasonal smoother length was set to the default value of 7.

The resulting residuals were subsequently post-processed to remove potential artefacts introduced during decomposition. Outliers were identified using the DBSCAN algorithm [Ester et al., 1996], a density-based clustering method. The maximum neighbourhood distance was set as *eps* = 0.5, and the minimum number of samples required to define a core point (including the point itself) was set to $DB_{min\_samples}$ = 5. To account for temporal proximity between observations, DBSCAN was applied in a

two-dimensional space defined by time and variable value. Thus, clustering required proximity in both dimensions. The Euclidean distance between two observations was computed according to [Eq. 2].

$$d = \sqrt{(DB_{ts}\Delta t)^2 + (\Delta x)^2} \quad \text{[Eq. 2]}$$

where Δt is the temporal separation between observations, Δx is the difference in the analysed variable (e.g., lake surface water temperature), and DB_{ts} is a temporal scaling factor defined as in [Eq. 3].

$$DB_{ts} = eps/STL_{period} \quad \text{[Eq. 3]}$$

This formulation ensures that temporal and magnitude differences are evaluated on comparable scales when defining density-based clusters. Consequently, observations exhibiting large magnitude changes over short time intervals are unlikely to satisfy the density criteria and are therefore classified as outliers, effectively constraining unrealistically steep short-term gradients.

6.2 Characteristics of anomalous mixing

We use the MixCI algorithm (Section 2.4) to define the stratification and overturning cycles in GBL. Being a cold monomictic lake, GBL typically mixes in summer when a thermocline with 4 °C (temperature of maximum density) would be present within the lake's area and is stratified during winter (Figure 11). Figure 12 presents the overturning and stratification cycles between 2005 and 2007, including the 2006 anomalous year, which had two periods of overturning instead of one extended period.

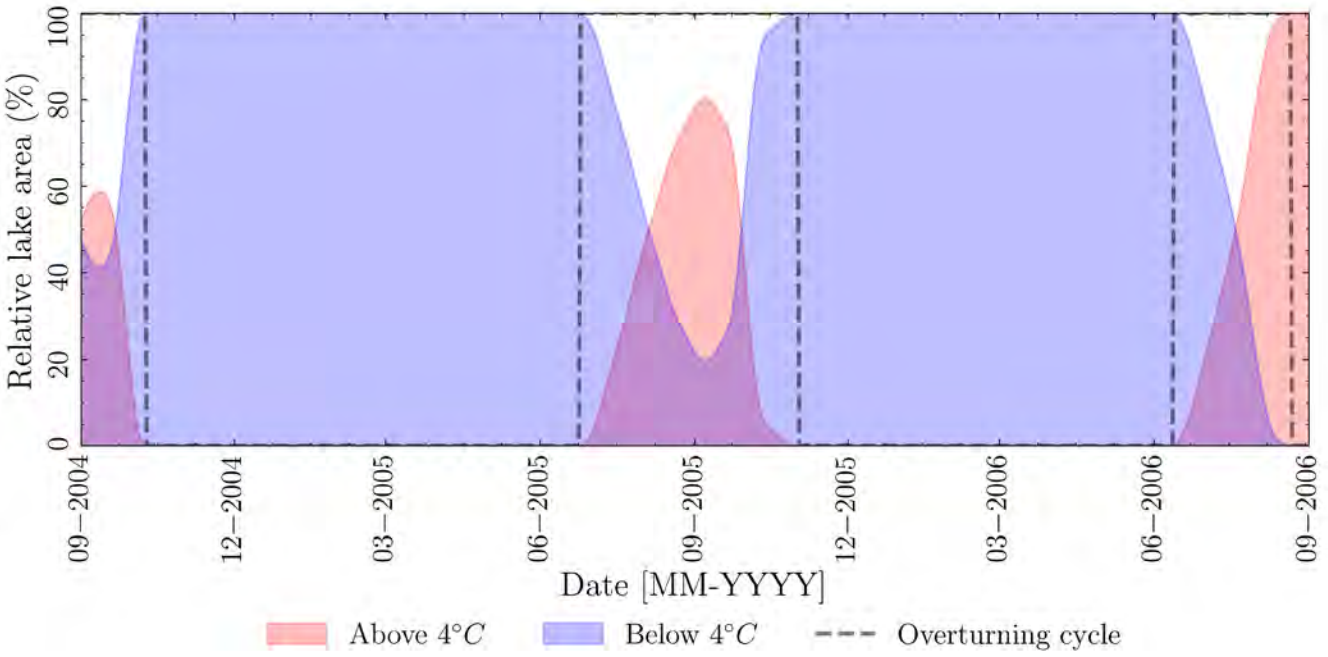

Figure 11: Stratification and overturning cycles for the entire lake centred on a normal year without contiguous summer stratification (2005). Lake areas with surface temperatures above 4 °C are shown in red, whereas areas below 4 °C are shown in blue.

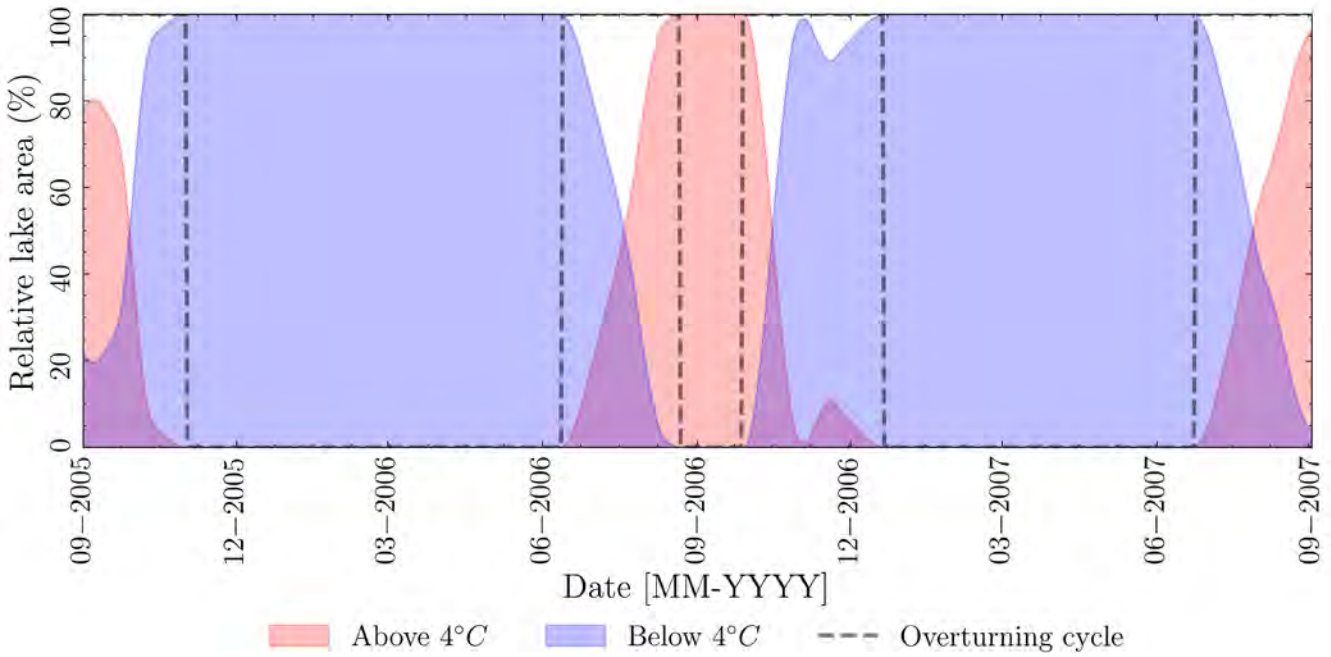

Figure 12: Stratification and overturning cycles for the entire lake cantered on an anomalous year with summer stratification in August/September (2006). Lake areas with surface temperatures above 4 °C are shown in red, whereas areas below 4 °C are shown in blue.

Statistical differences between anomalous and non-anomalous years were assessed using the two-sided Mann–Whitney U test, followed by the calculation of the probability of superiority (*PS*). Because anomalous years exhibit two overturning cycles, we compared the onset of the first cycle and the end of the second cycle with the start and end of the single overturning cycle observed in non-anomalous years to ensure a direct comparison.

We detected significant differences for both the start and end of the overturning period. In anomalous years, the onset of overturning occurred earlier, marking the end of winter stratification, with a probability of superiority of 10% ($PS = 0.10$). Conversely, the end of the overturning period occurred later in anomalous years, marking the onset of next winter stratification, with $PS = 0.89$.

Additionally, the durations of the overturning cycles were compared. Neither the first nor the second overturning cycle in anomalous years differed significantly in length from the single overturning cycle observed in non-anomalous years. In contrast, summer stratification differed substantially between the two regimes, as it was only observed during anomalous years.

Once we identify anomalous mixing years, we can determine which lake variables show significant differences between anomalous and non-anomalous year. For example, Figure 13 presents the spatially and monthly averaged decomposed chl-*a* for the entire lake in June. The June chl-*a* anomaly was consistent throughout the time series, with anomalous years (red points) typically exhibiting lower concentrations than non-anomalous years (black points). Welch's ANOVA indicates significant differences among years, as all null hypotheses were rejected. Subsequent grouping of the data into anomalous and non-anomalous years, followed by the Games-Howell post-hoc test, revealed significant differences in June for both the entire lake and the shallow portion, and in July for the shallow portion only. This enables us to determine key months (or other time periods) and spatial regimes of importance.

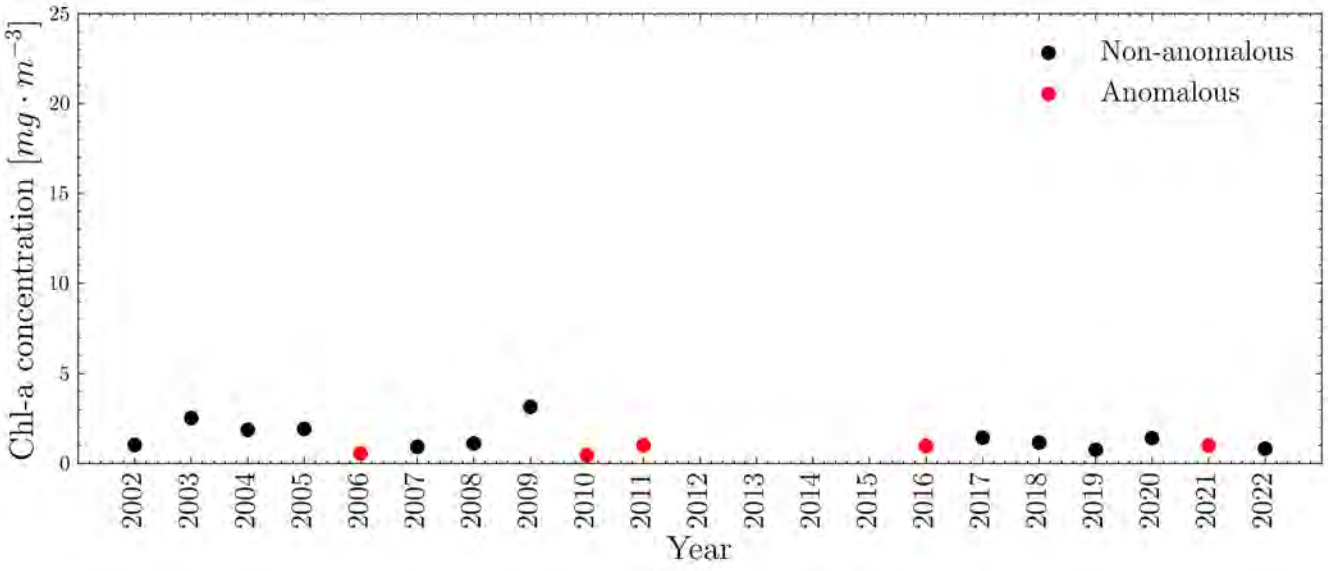

Figure 13: Spatially and temporally averaged chlorophyll-a concentration (chl-a) in June across the full time series for the entire lake.

6.3 Comparison of anomalous years to neighboring years

We use the gap-filled LSWT product (Section 2.1) which provides continuous spatial and temporal coverage from 2000 to 2022 for GBL. Figure 14 presents the spatially averaged daily raw LSWT for the entire lake. Higher temperatures were consistently observed in anomalous years compared with neighbouring years. For example, in 2006 (red), surface temperatures became non-null approximately 15 days earlier than in the preceding year (blue) and the subsequent year (orange). Moreover, positive temperatures were higher throughout the entire year, and persisted until November, which is atypical for this cold monomictic lake.

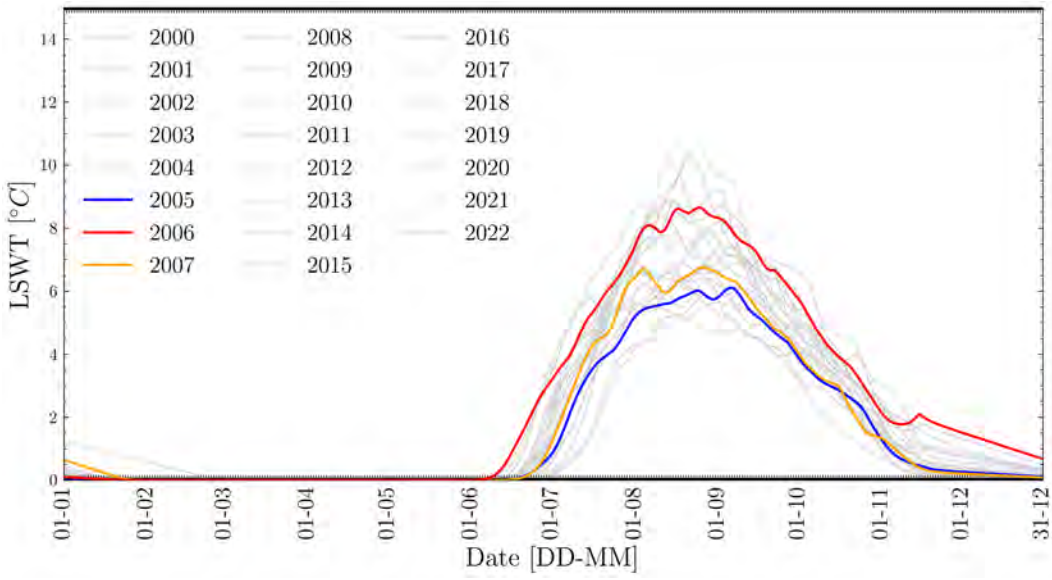

Figure 14: Spatially averaged daily lake surface water temperature (LSWT) for the entire lake. The red line represents an anomalous year, while the blue and orange lines denote the preceding and subsequent years, respectively.

After applying the pre-processing procedure, we performed Welch's ANOVA on monthly averaged LSWT residuals followed by the Games–Howell post-hoc test. For all months between June and October, Welch's ANOVA rejected the null hypothesis, indicating significant interannual differences in mean LSWT between anomalous and non-anomalous years. Temperatures from July through September were statistically higher in anomalous years than in non-anomalous years. For July, the statistical difference between anomalous and non-anomalous years was 0.4 °C. Despite the earlier onset of positive temperatures observed in Figure 14, the June monthly mean LSWT did not differ significantly between anomalous and non-anomalous years.

We spatially averaged the chl-*a* values according to lake bathymetry. Due to the time series gap between 2012 and 2015, we applied the seasonal and trend decomposition procedure independently to each of the two dataset periods. After removing the seasonal and trend components, the residual chl-*a* series was smoothed using an 8-day moving average to reduce short-term variability associated with physical processes (e.g., wind, air temperature) and biological fluctuations.

Figure 15 presents the spatially and 8-day time-averaged raw chl-*a* for the entire lake. In anomalous years (red time series), the late-spring chl-*a* peak is smaller than in neighbouring years (blue and orange time series). We hypothesize that this anomaly is due to variations in lake ice melt dynamics, which typically begin in mid-May [Kang et al., 2012; Carmack et al., 2024], and to associated reductions in ice thickness that allow earlier sunlight penetration, potentially increasing the annual heat budget [Carmack et al., 2024]. Notably, in some anomalous years, non-zero surface temperatures began approximately 15 days earlier than in non-anomalous years (Figure 14), which ends the winter stratification sooner in anomalous years (c.f. Figure 11 and Figure 12), which supports this hypothesis. This effect was primarily observed in June; during summer, chl-*a* concentrations stabilized at low levels, with further increases occurring in late September.

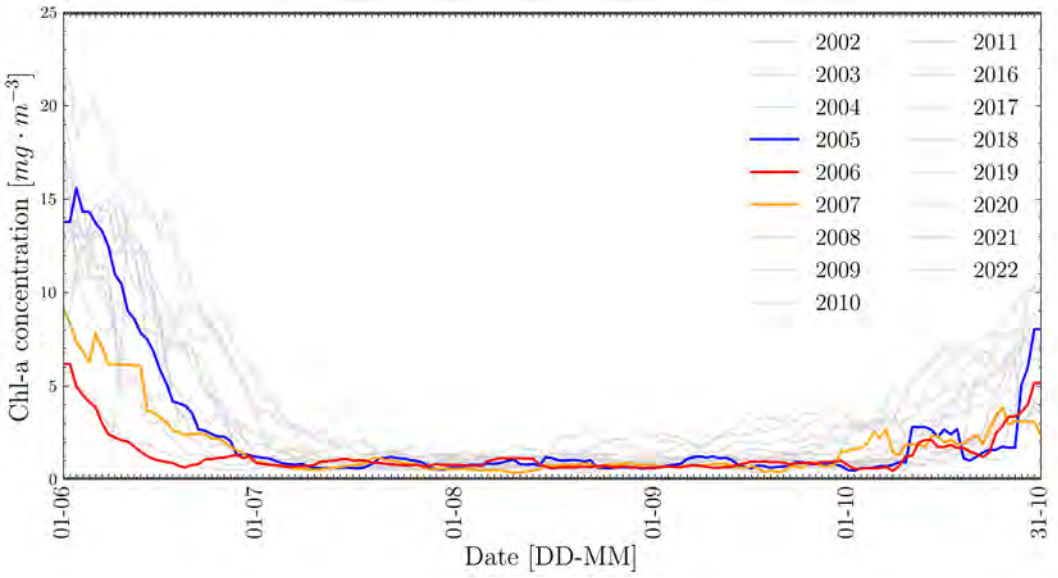

Figure 15: Spatially and 8-day time-averaged raw chlorophyll-a concentration (chl-a) for the entire lake. The red line represents an anomalous year, while the blue and orange lines denote the preceding and subsequent years, respectively.

7 References

Adrian, R., O'Reilly, C. M., Zagarese, H., Baines, S. B., Hessen, D. O., Keller, W., Livingstone, D. M., Sommaruga, R., Straile, D., Van Donk, E., Weyhenmeyer, G. A., & Winder, M. (2009). Lakes as sentinels of climate change. *Limnology and Oceanography*, *54*(6part2), 2283–2297. https://doi.org/10.4319/lo.2009.54.6_part_2.2283

Andersen, T., Carstensen, J., Hernández-García, E., & Duarte, C. M. (2009). Ecological thresholds and regime shifts: Approaches to identification. Trends in Ecology & Evolution, 24(1), 49–57. https://doi.org/10.1016/j.tree.2008.07.014

Armstrong McKay, D. I., Staal, A., Abrams, J. F., Winkelmann, R., Sakschewski, B., Loriani, S., Fetzer, I., Cornell, S. E., Rockström, J., & Lenton, T. M. (2022). Exceeding 1.5°C global warming could trigger multiple climate tipping points. Science, 377(6611), eabn7950. https://doi.org/10.1126/science.abn7950 Basu, A., Culpepper, J., Blagrave, K., & Sharma, S. (2024). Phenological Shifts in Lake Ice Cover Across the Northern Hemisphere: A Glimpse Into the Past, Present, and the Future of Lake Ice Phenology. *Water Resources Research*, *60*(9), e2023WR036392. https://doi.org/10.1029/2023WR036392

Calmettes, B., Simis, S, X. Liu, Cretaux JF, Carrea L, H. Yésou, C. Duguay, J. Murfitt, A. Mangelli, C. Fatras, L. Iris. 2025. Lakes Climate Change Initiative Product Specification Document (PSD), version 3.0.0. European Space Agency.

Carmack, E., Vagle, S., Kheyrollah Pour, H., 2024. Seasonal Temperature and Circulation Patterns in a Hybrid Polar Lake, Great Bear Lake, Canada. Journal of Geophysical Research: Earth Surface 129, e2024JF007650. https://doi.org/10.1029/2024JF007650

Carrea, L., Crétaux, J.-F., Liu, X., Wu, Y., Bergé-Nguyen, M., Calmettes, B., Duguay, C., Jiang, D., Merchant, C.J., Mueller, D., Selmes, N., Simis, S., Spyrakos, E., Stelzer, K., Warren, M., Yesou, H., Zhang, D., 2024. ESA Lakes Climate Change Initiative (Lakes_cci): Lake products, Version 2.1. https://doi.org/10.5285/7FC9DF8070D34CACAB8092E45EF276F1

Cleveland, R.B., Cleveland, W.S., McRae, J.E., Terpenning, I., 1990. STL: A seasonal-trend decomposition. Journal of Official Statistics 6, 3–73.

Ester, M., Kriegel, H.-P., Sander, J., Xu, X., 1996. A Density-Based Algorithm for Discovering Clusters in Large Spatial Databases with Noise, in: Proceedings of the 2nd International Conference on Knowledge Discovery and Data Mining. Presented at the International Conference on Knowledge Discovery and Data Mining, AAAI Press, Portland, pp. 226–231.

Games, P.A., Howell, J.F., 1976. Pairwise Multiple Comparison Procedures with Unequal N's and/or Variances: A Monte Carlo Study. Journal of Educational Statistics 1, 113–125. https://doi.org/10.2307/1164979

Gilarranz, L. J., Narwani, A., Odermatt, D., Siber, R., & Dakos, V. (2022). Regime shifts, trends, and variability of lake productivity at a global scale. *Proceedings of the National Academy of Sciences*, *119*(35), e2116413119. https://doi.org/10.1073/pnas.2116413119

Golub, M., Thiery, W., Marcé, R., Pierson, D., Vanderkelen, I., Mercado-Bettin, D., Woolway, R. I., Grant, L., Jennings, E., Kraemer, B. M., Schewe, J., Zhao, F., Frieler, K., Mengel, M., Bogomolov, V. Y., Bouffard, D., Côté, M., Couture, R.-M., Debolskiy, A. V., Droppers, B., Gal, G., Guo, M., Janssen, A. B. G., Kirillin, G., Ladwig, R., Magee, M., Moore, T., Perroud, M., Piccolroaz, S., Raaman Vinnaa, L., Schmid, M., Shatwell, T., Stepanenko, V. M., Tan, Z., Woodward, B., Yao, H., Adrian, R., Allan, M., Anneville, O., Arvola, L., Atkins, K., Boegman, L., Carey, C., Christianson, K., de Eyto, E., DeGasperi, C., Grechushnikova, M., Hejzlar, J., Joehnk, K., Jones, I. D., Laas, A., Mackay, E. B., Mammarella, I.,

Markensten, H., McBride, C., Özkundakci, D., Potes, M., Rinke, K., Robertson, D., Rusak, J. A., Salgado, R., van der Linden , L., Verburg, P., Wain, D., Ward, N. K., Wollrab, S., and Zdorovennova, G.: A framework for ensemble modelling of climate change impacts on lakes worldwide: the ISIMIP Lake Sector, Geosci. Model Dev., 15, 4597–4623, https://doi.org/10.5194/gmd-15-4597-2022, 2022.

Gray, J., Sulla-Menashe, D., & Friedl, M. A. (2019). *User Guide to Collection 6 MODIS Land Cover Dynamics (MCD12Q2) Product*. NASA.

Groom S. et al. (2024). Ocean Colour Climate Change Initiative Product User Guide for v6.0 Dataset. Version 6.5. European Space Agency. http://www.esa-oceancolour-cci.org/

Johnson, L., 1966. Temperature of Maximum Density of Fresh Water and its Effect on Circulation in Great Bear Lake. J. Fish. Res. Bd. Can. 23, 963–973. https://doi.org/10.1139/f66-089

Kang, K.-K., Duguay, C.R., Howell, S.E.L., 2012. Estimating ice phenology on large northern lakes from AMSR-E: algorithm development and application to Great Bear Lake and Great Slave Lake, Canada. The Cryosphere 6, 235–254. https://doi.org/10.5194/tc-6-235-2012

Khazaei, B., Read, L. K., Casali, M., Sampson, K. M., and Yates, D. N.: GLOBathy, the global lakes bathymetry dataset, Sci. Data, 9, 36, https://doi.org/10.1038/s41597-022-01132-9, 2022.

Lehmann, E.L., Romano, J.P., 2022. Testing Statistical Hypotheses, Springer Texts in Statistics. Springer International Publishing, Cham. https://doi.org/10.1007/978-3-030-70578-7

Lenton, T. M., Abrams, J. F., Bartsch, A., Bathiany, S., Boulton, C. A., Buxton, J. E., Conversi, A., Cunliffe, A. M., Hebden, S., Lavergne, T., Poulter, B., Shepherd, A., Smith, T., Swingedouw, D., Winkelmann, R., & Boers, N. (2024). Remotely sensing potential climate change tipping points across scales. *Nature Communications*, *15*(1), 343. https://doi.org/10.1038/s41467-023-44609-w

Levermann, A., Bamber, J. L., Drijfhout, S., Ganopolski, A., Haeberli, W., Harris, N. R. P., Huss, M., Krüger, K., Lenton, T. M., Lindsay, R. W., Notz, D., Wadhams, P., & Weber, S. (2012). Potential climatic transitions with profound impact on Europe: Review of the current state of six 'tipping elements of the climate system.' *Climatic Change*, *110*(3–4), 845–878. https://doi.org/10.1007/s10584-011-0126-5

Liu, X., Simis, S., Calmettes, B., Duguay, C., Merchant, C., Carrea, L., Crétaux, J.-F., 2024. D4.3. Product User Guide (PUG) (No. CCI-LAKES2- 0021- PUG). European Space Agency.

Loriani, S., Bartsch, A., Calamita, E., Donges, J. F., Hebden, S., Hirota, M., Landolfi, A., Nagler, T., Sakschewski, B., Staal, A., Verbesselt, J., Winkelmann, R., Wood, R., & Wunderling, N. (2025). Monitoring the Multiple Stages of Climate Tipping Systems from Space: Do the GCOS Essential Climate Variables Meet the Needs? *Surveys in Geophysics*, *46*(2), 327–374. https://doi.org/10.1007/s10712-024-09866-4

MacCallum, S. N., & Merchant, C. J. (2012). Surface water temperature observations of large lakes by optimal estimation. *Canadian Journal of Remote Sensing*, *38*(1), 25–45. https://doi.org/10.5589/m12-010

Messager, M. L., Lehner, B., Grill, G., Nedeva, I., and Schmitt, O.: Estimating the volume and age of water stored in global lakes using a geo-statistical approach, Nat. Commun., 7, 13603, https://doi.org/10.1038/ncomms13603, 2016.

Moore, T. S., Campbell, J. W., & Feng, H. (2001). A fuzzy logic classification scheme for selecting and blending satellite ocean color algorithms. *IEEE Transactions on Geoscience and Remote Sensing*, *39*(8), 1764–1776. https://doi.org/10.1109/36.942555

Scheffer, M., Bascompte, J., Brock, W. A., Brovkin, V., Carpenter, S. R., Dakos, V., Held, H., Van Nes, E. H., Rietkerk, M., & Sugihara, G. (2009). Early-warning signals for critical transitions. *Nature*, *461*(7260), 53–59. https://doi.org/10.1038/nature08227.

Simis, S., Carrea, L., Calmettes, B., Crétaux, J-F., Duguay, C., C. Fatras, Liu, X., Mangili, A. Müller, D., Yésou, H. 2025. Lakes Climate Change Initiative Algorithm Theoretical Basis Document (ATBD), version 3.0.0. European Space Agency. DOI: 10.5281/zenodo.17288453

Simis, S., Carrea, L., Calmettes, B., Crétaux, J-F., Duguay, C., Fatras, C., Jiang, D., Liu, X., Mangilli, A., Merchant, C., Mueller, D., Spyrakos, E., Yésou, H. 2025. Lakes Climate Change Initiative Product Validation and Intercomparison Report (PVIR), version 3.0.0. European Space Agency. DOI: 10.5281/zenodo.18234692

Tan, Z., Yao, H., Melack, J., Grossart, H.-P., Jansen, J., Balathandayuthabani, S., Sargsyan, K., & Leung, L. R. (2024). A Lake Biogeochemistry Model for Global Methane Emissions: Model Development, Site-Level Validation, and Global Applicability. *Journal of Advances in Modeling Earth Systems*, *16*(10), e2024MS004275. https://doi.org/10.1029/2024MS004275

Woolway, R. I., & Merchant, C. J. (2019). Worldwide alteration of lake mixing regimes in response to climate change. *Nature Geoscience*, *12*(4), 271–276. https://doi.org/10.1038/s41561-019-0322-x